Chemical Engineering Journal 145 (2009) 385–392

Contents lists available at ScienceDirect

Chemical Engineering Journal

journal homepage: www.elsevier.com/locate/cej

Oxidative dehydrogenation of ethane in an electrochemical packed-bed membrane reactor: Model and experimental validation

Lyubomir Chalakov[a], Liisa K. Rihko-Struckmann[b,*], Barbara Munder[b], Kai Sundmacher[a,b]

[a] Otto-von-Guericke University Magdeburg, Process Systems Engineering, Universitätsplatz 2, D-39106 Magdeburg, Germany
[b] Max Planck Institute for Dynamics of Complex Technical Systems, Sandtorstrasse 1, D-39106 Magdeburg, Germany

ARTICLE INFO

Article history:
Received 8 November 2007
Received in revised form 15 August 2008
Accepted 18 August 2008

Keywords:
Ethane oxidative dehydrogenation
Electrochemical membrane reactor
Modelling

ABSTRACT

A model was developed for the electrochemical oxidative dehydrogenation of ethane to ethylene in a solid electrolyte membrane reactor. Experimental data from the process with oxygen being supplied either electrochemically or gaseously were used in the model validation. In the model description, the converse axial distribution of the oxygen concentration in the reactor operated in the co-feed modus as well as in the electrochemical membrane modus was taken into account. The conversion of ethane and the selectivity to the desired product ethylene were well predicted with the model that included the kinetic equations based upon the Mars-van-Krevelen or the Langmuir-Hinshelwood mechanisms for investigations in the co-feed modus with gaseous dioxygen. This model was not directly applicable for the conditions of an electrochemical membrane reactor. The kinetics of the oxygen reduction on the cathode, the transfer of oxygen ions from the cathode to the anode, as well as the formation of the gaseous dioxygen on the anode, were therefore included in the model. Furthermore, the model for the electrochemical operation was extended by two additional side reactions that describe the electrochemically induced oxidation of the intermediate ethylene. After this, the experimental data measured in the temperature range of 540–620 °C agreed well with the predictions of the extended model.

1. Introduction

Ethylene and propylene are industrially the most important olefins. Due to the relative high reactivities, only limited amounts of them exist in natural gas or crude oil. Thus, they must be manufactured by cracking processes. Ethylene is mostly produced by thermal cracking of petroleum hydrocarbons with steam. The process is called steam cracking or pyrolysis and it is carried out at temperatures above 750 °C [1]. Alternative methods for ethylene production have not yet been commercialised, but there is a growing research interest in this field. One alternative method is the heterogeneously catalysed oxidative dehydrogenation of ethane (ODHE). During the last few years, several new and promising catalysts for this process have been found, and they have enabled high activity and selectivity at relative low temperatures. The insufficient selectivity could also be surmounted using highly active materials. Cavani et al. [2] summarized several catalytic materials being active in this reaction in their overview, but recently, completely new materials or novel modifications of well known former catalysts have been presented. Heracleous et al. [3,4], for example, tested Ni-Nb-O mixed oxides that exhibited both a high activity in ODHE and a very high ethylene selectivity (~90%) with an overall ethylene yield of 46% at 400 °C. The supported and unsupported vanadium oxides, often mixed with other metal oxides, are active at temperatures between 300 and 600 °C. Botella et al. [5] obtained selectivities higher than 80% at ethane conversion levels higher than 80%, while operating at relatively low reaction temperatures (340–400 °C) with an MoVTeNbO catalyst. Solsona et al. [6] found in their study that V-containing catalysts are approximately four times more active than pure Mo-catalyst, whereas a Mo-V-containing catalyst was the most selective one for ethylene in the ODHE. The reaction has also been investigated by Klisinska et al. [7] with VO_x/SiO_2 (VSi) and VO_x/MgO (VMg) catalysts which were doped with various additives from the main group elements (K and P) and transition metal ions (Ni, Cr, Nb, and Mo). Although the earlier mentioned mixed oxides might show slightly higher activities and selectivities in ODHE compared to the well-known vanadia containing catalysts, the latter was selected in the present study because this type of catalyst has been largely used, it has been detailed characterised, and it is simple to synthesise by impregnation [8]. In the present study we applied the alumina-supported vanadium oxide catalyst $VO_x/\gamma\text{-}Al_2O_3$, as used also in several earlier alkane dehydrogenation investigations [9,10].

* Corresponding author. Tel.: +49 391 6110318; fax: +49 391 6110566.
E-mail address: rihko@mpi-magdeburg.mpg.de (L.K. Rihko-Struckmann).

1385-8947/$ – see front matter © 2008 Elsevier B.V. All rights reserved.
doi:10.1016/j.cej.2008.08.017

Aside from the optimal catalyst selection, the type of the applied reactor is another important factor required for the maximisation of the yield of one intermediate. For the ODHE to ethylene, various reactor types have been implemented. Martinez-Huerta et al. [11] carried out ethane ODH in a conventional isothermal fixed-bed reactor in the temperature range of 450–610 °C at atmospheric pressure. The operation of a classical packed-bed reactor was compared to that of a packed-bed membrane reactor (PBMR) by Klose et al. [12]. The PBMR with an inert, porous ceramic alumina composite membrane, filled with VO_x/γ-Al_2O_3 catalysts (1.4% V) showed a higher selectivity towards the desired product, ethylene, at higher conversion level for the ODHE reaction in comparison to the corresponding packed-bed reactor. Using the same catalyst, Ahchieva et al. [13] could significantly improve the selectivity to ethylene in a pilot scale fluidized bed membrane reactor (FLBMR) compared to the corresponding conventional fluidized bed reactor (FLBR).

Electrochemical membrane reactors (EMR) equipped with gas dense membranes [14] are promising reactor solutions, especially the ones with oxygen ion conducting membranes [15,16]. In our previous study, an yttria stabilized zirconia (YSZ) membrane was applied in a tubular packed-bed membrane reactor with a membrane/electrode composition of Au|YSZ|Pt [17], and where the anodic compartment was filled with VO_x/γ-Al_2O_3 catalyst particles. The working principle of an EMR is comparable to that of a solid-oxide fuel cell (SOFC), with the difference that in a fuel cell the on-going reactions on the electrodes generate the electric potential difference between the anode and cathode. In EMR, operating at lower temperatures than SOFC, the current between the electrodes is usually supported additionally with applied electric potential (oxygen pumping). On the cathode, oxygen is reduced to oxygen anions. These anions are transported through the ceramic membrane to the anode compartment, where diluted ethane is fed. Ethane reacts with the supplied oxygen species to form ethylene and CO_x, and the released electrons are transported back to the cathode via the outer electric circuit. The oxygen transferred across the membrane can be precisely controlled by the applied electric potential or current between the two electrodes. Fig. 1 shows the schematic diagram of an EMR.

In our recent publication [17], the feasibility of electrochemical ethane dehydrogenation was demonstrated, and a comparison of the EMR and packed-bed reactor (PBR) operation mode was carried out. Based upon the achieved experimental results, it was concluded that a model based analysis is necessary for the improvement of the reactor performance and the optimisation of the operation parameters. Therefore, the goal of the present study is to develop a model which is able to describe the behaviour of the electrochemical membrane reactor during the oxidative dehydrogenation of ethane to ethylene. The experimental data obtained using the electrochemical membrane reactor [17] will be analysed in detail, and an extended reactor model including the kinetic equations and the respective parameters will be presented.

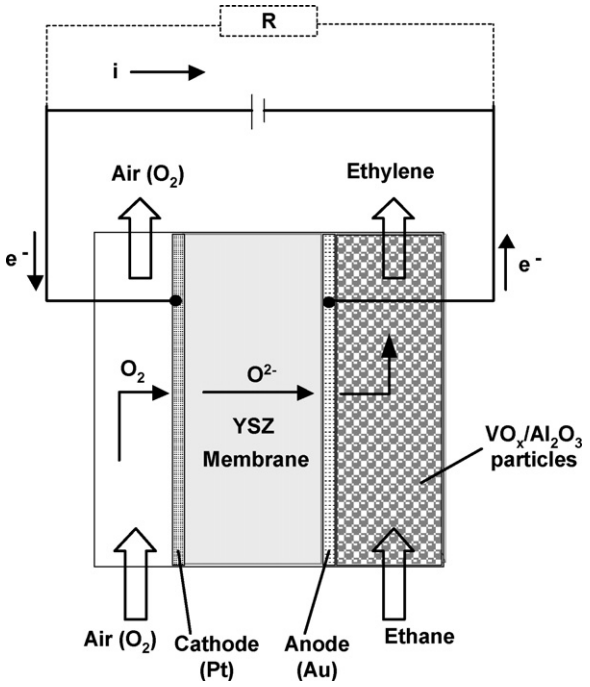

Fig. 1. Shematic illustration of ethane oxidative dehydrogenation in an electrochemical membrane reactor.

2. Kinetics of ODH reactions

In literature, only few papers consider the kinetic aspects of the ODHE reaction. A detailed overview regarding the proposed kinetic models for C_2–C_3 alkanes ODH on oxide catalysts was recently given by Grabowski [18]. Supported vanadia catalysts were used in all here reviewed studies. Oyama et al. [19], Grabowski and Sloczynski [20] and Le Bars et al. [21] proposed kinetic models and reaction networks based upon the experimental results achieved using either VO_x/SiO_2 catalyst undoped or the same catalyst doped with potassium. Rao and Deo [22] investigated the effects of vanadia surface loading on the ODH reaction kinetics with supported VO_x/TiO_2 catalysts. Klose et al. [23] performed studies, where the ODHE was carried out by applying a VO_x/γ-Al_2O_3 catalyst. All authors used a parallel-consecutive reaction network in their kinetic analysis for the description of the ODHE system. Generally, the formation of an ethoxy complex was proposed to be the first step of the ODH reaction of ethane, but depending on the system various successive stages were proposed. However, each of the models is valid only for specific operation conditions.

In this study, we found the kinetic model proposed by Klose et al. [23] as the most suitable one for our reaction system. In the reaction network (see Fig. 2), ethane reacts following two parallel pathways to form ethylene and CO_2 in accordance with Eqs. (1) and (2).

$$C_2H_6 + 0.5O_2 \rightarrow C_2H_4 + H_2O \quad (1)$$

$$C_2H_6 + 3.5O_2 \rightarrow 2CO_2 + 3H_2O \quad (2)$$

The formed ethylene can be further oxidized through another two parallel pathways to CO or CO_2 according to Eqs. (3) and (4).

$$C_2H_4 + 2O_2 \rightarrow 2CO + 2H_2O \quad (3)$$

$$C_2H_4 + 3O_2 \rightarrow 2CO_2 + 2H_2O \quad (4)$$

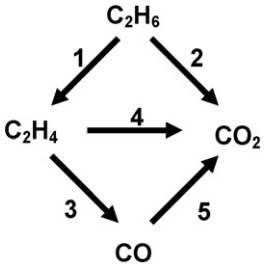

Fig. 2. Simplified reaction network for the oxidative dehydrogenation of ethane (ODHE).

Finally, the consecutive CO oxidation to CO_2 (Eq. (5)) also can take place.

$$CO + 0.5O_2 \rightarrow CO_2 \quad (5)$$

For the dehydrogenation step the Mars van Krevelen mechanism is assumed, where ethane reacts with the lattice oxygen of the catalyst to form ethylene. The reduced catalyst is subsequently reoxidized by gaseous oxygen

$$Cat_{red} + 0.5O_2 \rightarrow Cat_{ox} \quad (6)$$

which is supplied either electrochemically (see next chapter) or gaseously.

The total oxidation of ethane or ethylene (reactions (2)–(4)) is assumed to occur only in the presence of gaseous oxygen by the Langmuir-Hinshelwood mechanism, assuming a non-competitive adsorption of the reactants. The oxidation of CO (Eq. (5)) is also described by a Langmuir-Hinshelwood mechanism with competitive adsorption of the reactants. In accordance with the model presented by Klose et al. [23], we assumed that the oxygen participates in the dissociated form in all of the reactions with a reaction order in the kinetic equations of 0.5, whereas the reaction orders for all other compounds are considered to be one.

3. Kinetics of electrochemical reactions

The initial set of kinetic equations was extended by two additional equations for reactions (Eqs. (7) and (8)) describing the electrochemical oxygen reduction on the cathode and the release on the anode.

Cathode:

$$0.5O_2 + 2e^- \rightleftarrows O^{2-} \quad (7)$$

Anode:

$$O^{2-} \rightleftarrows 0.5O_2 + 2e^- \quad (8)$$

Such a similar electrochemical extension was also made in the model of EMR proposed by Munder et al. [24] for the electrochemically supported synthesis of maleic anhydride. The oxygen supply occurs due to the potential difference over the membrane via the conduction of oxygen anions (O^{2-}) in the fluorite-type solid electrolyte membrane (YSZ). At high temperatures, oxygen anions migrate from the cathode to the anode through the membrane, and the released electrons (e^-) are returned back to the cathode via the outer electric circuit. By increasing the potential difference between the electrodes with an external electric source, the oxygen transfer can be enhanced. In the EMR reactor, the anodic electrode surface is supplied with O^{2-} and, eventually, with other electrochemical oxygen species like O_2^-, O_2^{2-}, O^-, and the anodic compartment with gaseous O_2, formed on the anode. The heterogeneously catalysed reactions between gaseous dioxygen and the hydrocarbons are assumed to take place on the surface of the catalyst particles in the anodic compartment.

The electrochemical reaction steps (Eqs. (7) and (8)) are described by the Butler-Volmer kinetics (Eq. (9), valid for both electrodes). The forward and backward electrochemical charge transfer reactions taking place on both the anode and cathode are taken into consideration in the model.

$$r_{el}^{A/C} = k_0^{A/C} \exp\left(-\frac{E_A^{A/C}}{RT}\right)\left[\exp\left(\frac{\alpha_a^{A/C} F}{RT}\Delta\Phi^{A/C}\right) - \left(y_{O_2}\right)^{0.5} \times \exp\left(-\frac{\alpha_c^{A/C} F}{RT}\Delta\Phi^{A/C}\right)\right] \quad (9)$$

4. Electrochemical membrane reactor model

Our recently published experimental results [17] and additional unpublished data were used to determine the numeric values for the kinetic parameters. The details of the experimental set-up and conditions are given in [17] and are, therefore, only briefly summarized below. The experiments were performed in a tubular Au|YSZ|Pt packed-bed membrane reactor with a VO_x/γ-Al_2O_3 (1.4% V-content) catalyst bed. The thickness of the solid electrolyte membrane (13 mol% YSZ) was 0.5 mm and the electrode area was 25.7 cm^2. The reactor was operated either in a co-feed or in an electrochemical membrane reactor mode at atmospheric pressure. In the co-feed mode, both gaseous reactants – diluted ethane and oxygen – were delivered directly into the anodic compartment, and the reactor practically operated as a conventional gas phase plug flow packed-bed reactor. In the EMR mode, the oxygen was applied electrochemically through the membrane. The relation between the oxygen transfer flux (J) of one oxygen ion, O^{2-}, and the current (I) is given by the Faraday law: $J = I/2F$, where F is the Faraday constant. In the present study, the current was gradually increased in 10 mA intervals in the range of 0.002–0.1 A. As an example, with the volumetric flow on the anodic side of 100 ml/min (7.44×10^{-5} mol/s) and ethane concentration 0.111 vol-%, a total current of 50 mA gives a molar oxygen flow of 1.30×10^{-7} mol/s, corresponding to a oxygen/ethane molar ratio of 1.57. The applied oxygen/ethane molar ratio was in the range of 0.18–3.10 (PBR), resp. 0.06–3.10 (EMR), during the experiments. The investigations were typically carried out in the temperature range of 500–620 °C. The main products of the investigated ODHE reaction were ethylene, CO and CO_2. The formation of carbonaceous deposits was negligible under the conditions discussed in this paper. A formation of carbonaceous deposits was observed in EMR experiments without oxygen supply. For all the presented experimental data, the carbon balance that had been calculated on the basis of these three main products was always ≥95%.

The most important findings in this experimental study were that the ethane total conversion was higher, while the ethylene selectivity was not positively influenced during the operation of the electrochemical membrane reactor in comparison to the operation of the packed-bed membrane reactor [17]. The selectivity ratio S_{CO_2}/S_{CO} was found to depend upon the type of oxygen supply provided in such a way that when providing a gaseous dioxygen supply, the ratio was always lower than that determined through the use of an electrochemical oxygen supply. In order to analyse these results, the above kinetic model for the oxidative dehydrogenation of ethane to ethylene was integrated to a reactor model which had been developed by Munder et al. [24] to describe the prevailing physical phenomena in an electrochemical solid electrolyte membrane reactor (SEMR). The developed model had been investigated by Munder et al. [24,25] using the partial oxidation of *n*-butane to maleic anhydride as a model reaction. Therefore, the existing model was here modified to our reaction system (the anodic compartment filled with catalyst particles of VO_x/γ-Al_2O_3). The main assumptions made in the model are listed in the following chapter.

The anodic compartment of the reactor which had been filled with the catalyst is described by a one dimensional pseudohomogeneous approach, where possible radial concentration gradients have been neglected. The mass transport within the anodic compartment is dominated by convection and diffusion in the axial direction. Initially, we assumed that the cathodic side was a quasi-steady state oxygen reservoir and that the only electrochemical reaction on the anodic side was the release of gaseous dioxygen at the membrane–electrode interface. This means that the ODHE reactions occur non-electrochemically. Furthermore, it was assumed

that the reactor is operated under isothermal (due to the low educts concentration and the temperature control provided by the experimental set-up) and isobaric conditions, as well as that the gas phases obey the ideal gas law. More details about the model are given in [24]. The simulation environment DIVA 3.9 [26], a dynamic simulator for chemical engineering plants (University of Stuttgart, Germany), was used as the mathematical tool in the model simulations.

5. Analysis of experimental results and model validation

5.1. Electrochemical reactions

Initially, we took the parameter values for C^{YSZ} (YSZ conductivity constant), E_A^{YSZ} (activation energy for O^{2-} conduction within the YSZ membrane), $k_0^{A/C}$, $E_A^{A/C}$ and $\alpha^{A/C}$ for the electrochemical reactions (Eqs. (7) and (8)) directly from [24]. However, the model predictions of the characteristic isothermal current–voltage diagram with the parameters from [24] were not satisfying compared to our experimental measurements. This might be due to the high sensitivity of an electrochemical system to the membrane composition, the anodic and cathodic materials and the preparation techniques, as already previously reported in [27]. Moreover, the ageing of the reactor might also influence its operation. The reactor in this study was operated for about 100 h prior the present investigations. Some key differences between the reactor used in [24] and our reactor [17] are listed below. The different composition of the membrane material (13 wt-% vs. 10 wt-%, respectively) directly influences the oxygen conductivity, whereas the membrane in the present study (with its lower stabilisation degree) should possess a slightly decreased conductivity. The Pt–Ag alloy cathode used in the experimental study by Ye et al. [28] being the basis for the model in [24] could advance the oxygen reduction process on the cathode. The slightly different radial and axial dimensions of the reactors are considered in the model calculations.

The experimental current–voltage curve was ascertained under the following working conditions: temperature of 580 °C; flow rate of 100 ml/min; 0.1% C_2H_6, diluted in He in the anodic compartment and air in the cathodic compartment. The measurements were carried out without a reference electrode and therefore, the cathodic and the anodic charge transfer processes could not be measured separately. The construction of a reliable reference electrode in a solid electrolyte system, such as in a solid-oxide fuel cell, is highly challenging [29], and was not possible here. The ratio of the cathode to the anode current density exchange was therefore assumed to be 10, and the charge transfer coefficients equal, similarly as reported in [24]. Under the above mentioned assumptions, the activation energies for the electrochemical reactions, $E_A^{A/C}$, and the pre-exponential factor, C^{YSZ}, of the conductivity of the membrane, were re-estimated (see Table 1) and the calculated current–voltage curve is compared to the experimentally obtained data in Fig. 3.

Table 1
The estimated model parameters of the conductivity of the solid electrolyte and for the reactions of oxygen on both electrodes

Parameter	Value	Unit
C^{YSZ}	0.03×10^8	S K m^{-1}
E_A^{YSZ}	96.9×10^3 [a]	J mol^{-1}
k_0^A	1.46×10^3 [a]	mol m^{-2} s^{-1}
k_0^C	1.46×10^4 [a]	mol m^{-2} s^{-1}
$E_A^{A/C}$	130×10^3	J mol^{-1}
$\alpha^{A/C}$	0.3 [a]	–

[a] Munder et al. [24].

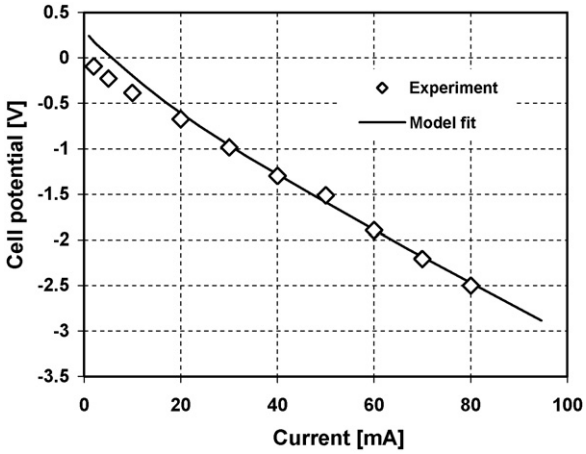

Fig. 3. Characteristic isothermal current–voltage curve of the EMR (T = 580 °C, W/F = 0.013 g min/cm^3, c_{Ethane} = 0.1 vol-%).

The limited conductivity of the membrane and non-optimal contact between the electrodes and the solid electrolyte hindered the investigations with higher hydrocarbon concentrations due to the limited supply of oxygen into the reaction anodic area. A possible solution for increasing the oxygen supply could be the more detailed optimisation of the electrode design. The current density in the membrane/electrode interface might be improved by the construction of a composite anode, where the solid electrolyte membrane, electron conducting electrode material and catalyst would be in a more close contact.

5.2. Heterogeneously catalysed reactions

The developed reactor model was first used to simulate the PBR behaviour in the ODHE with gaseous dioxygen without electrochemically supplied oxygen. In the investigations under conventional PBR conditions, the gaseous dioxygen was fed together with diluted ethane at one end of the reactor. The model predictions, including the kinetic parameters for the gas phase reactions (2)–(5) taken directly from literature [23], qualitatively agreed with our experimental results [17]. However, there was a slight deviation in the ethylene selectivity, as the model prediction was higher than the experimental observations. Furthermore, the calculated CO selectivity was lower than that experimentally observed, especially at low ethane conversions. The reason for the deviations might be due to the different operational conditions of the reactors. Klose et al. [23] used catalyst particles with a 10 times larger average particle diameter. Furthermore, they applied much lower catalyst/feed ratios and higher educt concentrations in comparison to our investigations. Therefore, in order to be able to better describe our experimental results in the PBR, the some kinetic parameters were re-estimated. In order to keep the number of re-estimations as small as possible, only the reaction rate coefficients were revalued by minimising the sum of the deviations between the experimental and modelled reactor output concentrations. Table 2 summarises all the kinetic parameters for the non-electrochemical reactions. Fig. 4 shows the model estimations, as well as the experimental results for ethane conversion and ethylene yield (a) and the ethylene, CO and CO_2 selectivity (b) as a function of the oxygen-to-ethane feed ratio. In general, a good agreement between the experimental results and the simulations was found after the parameter re-estimation, as the ethane conversion, ethylene yield and CO_2 selectivity were very well predicted. The model predicted the obtained experimental ethylene and CO selectivity most pre-

Table 2
The kinetic parameters of the heterogeneously catalysed gas phase reactions

Reaction	k_{0i}	$E_{A,i}$/kJ mol^{-1}
1-Ox	1.9×10^3 [mol kg^{-1} s^{-1}]	94[a]
1-Red	1.7×10^3 [mol$^{0.5}$ m$^{1.5}$ kg^{-1} s^{-1}]	94[a]
Reaction i (r_i)	k_{0i}/mol kg^{-1} s^{-1}	$E_{A,i}$/kJ mol^{-1}
$i=2$	4.4×10^3[a]	114[a]
$i=3$	19.6	51[a]
$i=4$	0.3[a]	51[a]
$i=5$	45.1×10^3	118[a]

[a] Klose et al. [23]

cisely in the interval of 1.0 and 1.5 for the oxygen-to-ethane feed ratio.

Subsequently, the parameters from Tables 1 and 2 were directly adopted for the simulation of the EMR operation conditions with electrochemically supplied oxygen. However, with this set of parameters it was not possible to satisfactorily predict the experimental results, as is illustrated in Fig. 5. The predicted selectivity and the yield to ethylene (as can be seen in Fig. 5) in the EMR modus, are high and the selectivity of the undesirable products CO_x low. Unfortunately, the experimental results in the EMR operation clearly deviated from the modelled results—much higher CO_x selectivity, as well as a much lower ethylene selectivity and yield were observed in the experiments as had been predicted by the model. Principally, the EMR and PBR are operated with clearly deviating oxygen profiles in the reactor. The oxygen pumping in the EMR operating mode provides a controlled and even oxygen input over the whole catalyst bed, whereas in the PBR the local O_2/C_2H_4 ratio is high at the inlet of the reaction zone and decreases in the axial direction during the operation. However, the converse oxygen profiles in the EMR and PBR modus cannot be the explanation for the deviation between the experimental results and the calculated ones in EMR modus, as the different oxygen profiles are fully regarded in the model.

Therefore, it is more likely that there are additional, electrochemically induced side reactions, as had also been suggested in the maleic anhydride synthesis with solid electrolyte membrane [17,28]. Compared to the PBR mode, where the oxygen on the anode can only exist in the form of gaseous O_2, additional oxygen species could be present in the system, e.g. O^{2-}, O_2^-, O_2^{2-}, O^-, O (adsorbed) during electrochemical pumping in the EMR operation. Therefore, the final modification of the model is that two additional electrochemical side reactions are implemented in the reaction network. The charged oxygen species might be highly active in the oxidation reaction such as had been concluded in [17], and there exists the possibility that ethylene can easily react with O^{2-} either to CO (reaction (3el)) or CO_2 (reaction (4el)) according to equations:

$$C_2H_4 + 4O^{2-} \rightarrow 2CO + 8e^- + 2H_2O \quad (3el)$$

$$C_2H_4 + 6O^{2-} \rightarrow 2CO + 12e^- + 2H_2O \quad (4el)$$

The backward reactions were assumed to be unlikely here, and therefore, the kinetics of the reactions Eqs. (3el) and (4el) were described by the simple Tafel equation (Eq. (10)).

$$r_{el}^{CO/CO_2} = k_{el}^{CO/CO_2} \left[\exp\left(\frac{\alpha_a^A F}{RT} \Delta\Phi^A \right) \right] y_{C_2H_4}^A \quad (10)$$

The complete set of the kinetic equations is summarized in Table 3. The model predictions calculated with the extended model including the electrochemical side reactions are presented in Fig. 6.

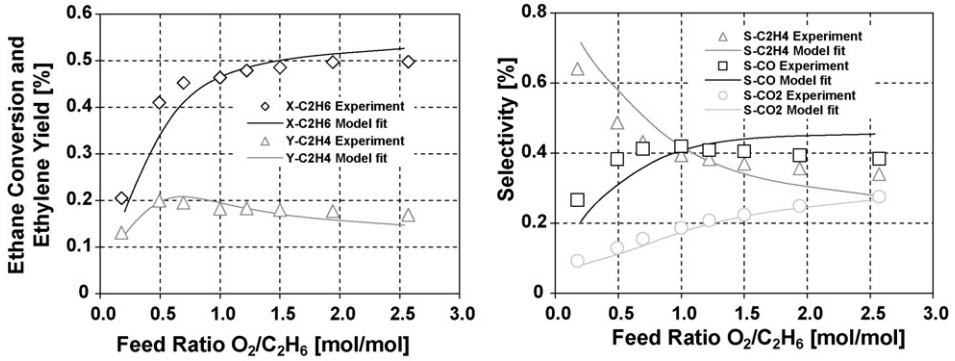

Fig. 4. Experimentally obtained and predicted ethane conversion, ethylene yield, and selectivities as a function of the oxygen-to-ethane feed ratio during PBR operation ($T = 580\,^\circ$C; $W/F = 0.013$ g min/cm^3).

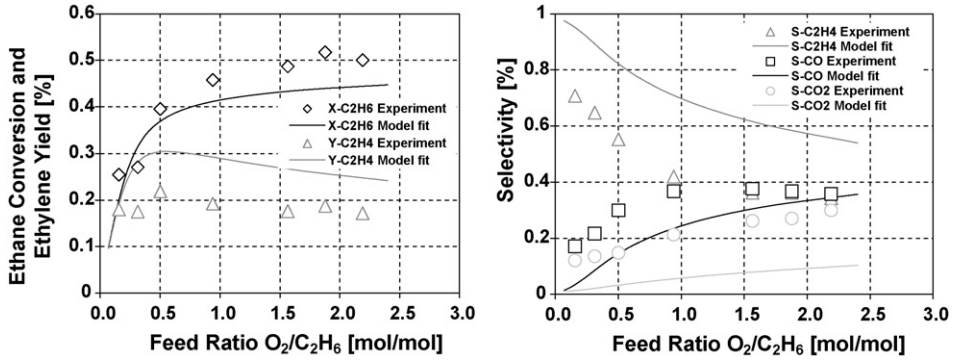

Fig. 5. Experimentally obtained and predicted ethane conversion, ethylene yield, and selectivities as function of the oxygen-to-ethane feed ratio during EMR operation ($T = 580\,^\circ$C; $W/F = 0.013$ g min/cm^3). The model predictions without the additional electrochemical reactions of ethylene.

Table 3
Kinetic equations for the reaction network

Reaction	Equation
(1)	$r_1 = \dfrac{k_{red} c_{C_2H_6} k_{ox} c_{O_2}^{0.5}}{k_{red} c_{C_2H_6} + k_{ox} c_{O_2}^{0.5}}$
(2)	$r_2 = k_2 \dfrac{K_{C_2H_6} c_{C_2H_6}}{\left[1 + K_{C_2H_6} c_{C_2H_6} + K_{CO_2} c_{CO_2}\right]} \times \dfrac{K_{O_2}^{0.5} c_{O_2}^{0.5}}{\left[1 + K_{O_2}^{0.5} c_{O_2}^{0.5}\right]}$
(3)	$r_3 = k_3 \dfrac{K_{C_2H_4} c_{C_2H_4}}{\left[1 + K_{C_2H_4} c_{C_2H_4} + K_{CO} c_{CO}\right]} \times \dfrac{K_{O_2}^{0.5} c_{O_2}^{0.5}}{\left[1 + K_{O_2}^{0.5} c_{O_2}^{0.5}\right]}$
(3el)	$r_{el}^{CO} = k_{el}^{CO} \left[\exp\left(\dfrac{\alpha_a^A F}{RT} \Delta\Phi^A\right)\right] y_{C_2H_4}^A$
(4)	$r_4 = k_4 \dfrac{K_{C_2H_4} c_{C_2H_4}}{\left[1 + K_{C_2H_4} c_{C_2H_4} + K_{CO_2} c_{CO_2}\right]} \times \dfrac{K_{O_2}^{0.5} c_{O_2}^{0.5}}{\left[1 + K_{O_2}^{0.5} c_{O_2}^{0.5}\right]}$
(4el)	$r_{el}^{CO_2} = k_{el}^{CO_2} \left[\exp\left(\dfrac{\alpha_a^A F}{RT} \Delta\Phi^A\right)\right] y_{C_2H_4}^A$
(5)	$r_5 = k_5 \dfrac{K_{CO} c_{CO} K_{O_2}^{0.5} c_{O_2}^{0.5}}{\left[1 + K_{CO} c_{CO} + K_{O_2}^{0.5} c_{O_2}^{0.5} + K_{CO_2} c_{CO_2}\right]^2}$
(6)	$r_{el}^C = k_0^C \exp\left(-\dfrac{E_A^C}{RT}\right) \left[\exp\left(\dfrac{\alpha_a^C F}{RT} \Delta\Phi^C\right) - (y_{O_2})^{0.5} \exp\left(-\dfrac{\alpha_c^C F}{RT} \Delta\Phi^C\right)\right]$
(7)	$r_{el}^A = k_0^A \exp\left(-\dfrac{E_A^A}{RT}\right) \left[\exp\left(\dfrac{\alpha_a^A F}{RT} \Delta\Phi^A\right) - (y_{O_2})^{0.5} \exp\left(-\dfrac{\alpha_c^A F}{RT} \Delta\Phi^A\right)\right]$

A good agreement between the experiments and the simulations was obtained with the following parameter values: the rate constants $k_{el}^{CO} = 1.1 \times 10^{-2}$ mol/m^2/s for reaction (3el) and $k_{el}^{CO_2} = 0.9 \times 10^{-2}$ mol/m^2/s for reaction (4el). The selectivity towards the three products, as well as the ethylene yield, were much better predicted with the final, extended model which considered the additional electrochemical oxidation reactions of the ethylene ((3el) and (4el)). Due to the oxygen consuming electrochemical side reactions, the reactions with ethane seem to be depressed to some extent. This might be the reason why the model prediction of the ethane conversion is limited even with this final form. The implementation of electrochemical side reactions in the model clearly improved its applicability, and the final extended model is able to describe the phenomena occurring in the anodic compartment in more detail. However, in this contribution the presented model is based on the apparent kinetics of the several catalytic and electrochemical reactions. Hence, in order to further improve the model one should conduct separate electrochemical measurements, and carry out detailed kinetic analysis of the heterogeneously catalysed reactions in order to enlighten the intrinsic kinetics of the various reactions in this complex network. Fig. 6c illustrates model predictions in a wider range of oxygen/ethane feed ratio. As seen in the illustration, the oxygen excess is expectedly increasing as a function of molar feed ratio. However, ethane conversion is not increasing considerably as more oxygen in provided, but the side reactions, the formation of carbon oxides, are more pronounced as oxygen concentration increases. The highest ethylene concentration is obtained at the oxygen/ethane molar ratio 0.55, which agreed well the experimental observations. At higher molar ratios, the ethylene concentration is steadily decreasing, and according to the model prediction it approaches zero at ratio 4.

Finally, we investigated the model predictions in various temperatures within the investigated temperature range by implementing the optimised activation energies $E_A^{CO\text{-}el}$ (220 kJ/mol) and $E_A^{CO_2\text{-}el}$ (180 kJ/mol) for the reactions (3el) and (4el). The activation energies for the non-electrochemical reactions were taken directly from literature [23], and the values are typical for catalytic reaction. The obtained activation energies (130 kJ/mol) for the electrochemical reactions ((6) and (7) in Table 1) are comparable as published

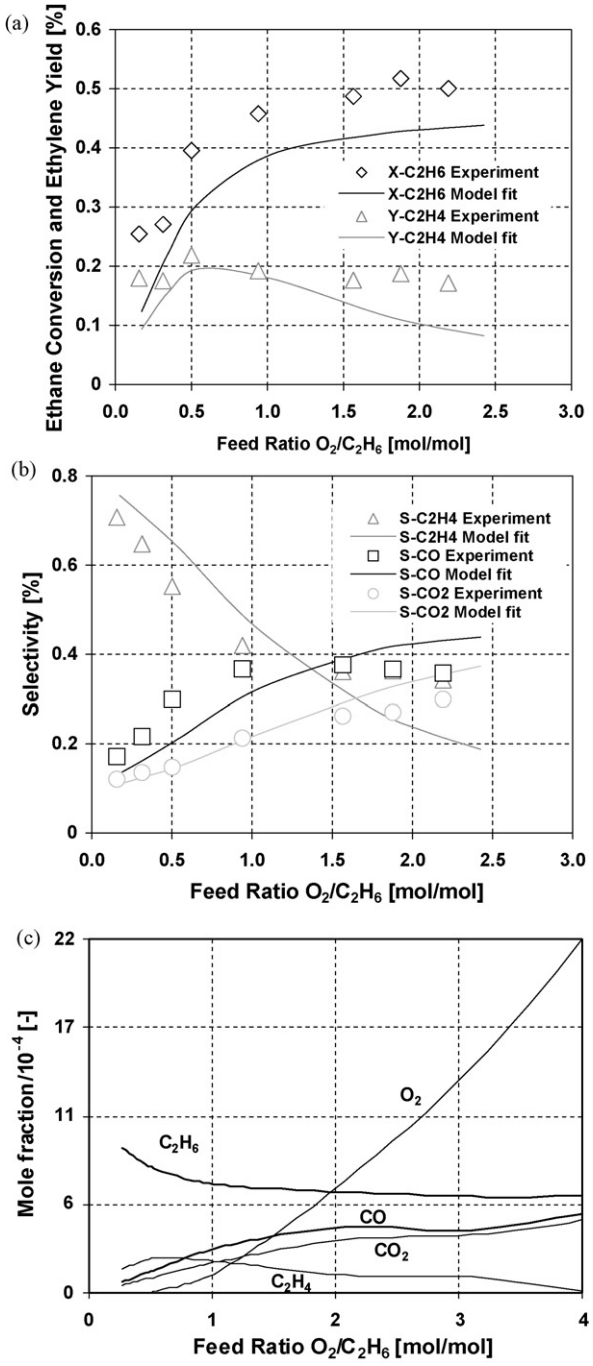

Fig. 6. Experimentally obtained and predicted ethane conversion (a), ethylene yield (a), and selectivities (b) as a function of the oxygen-to-ethane feed ratio during EMR operation (T = 580 °C; W/F = 0.013 g min/cm^3). The predicted molar concentrations at initial oxygen/ethane molar ratio between 0.25 and 4.0 (c). All predicted values calculated with the extended model including the additional electrochemical side reactions.

for electrochemical reactions in the anode and cathode in SOFC fuel cells (120 and 100 kJ/mol [30]). The activation energy values of the electrochemical side reactions (3el) and (4el) are higher than the other ones in Table 2, increasing the influence of the reactions at high temperatures. The dependence of the product selectivity and ethylene yield as a function of the reaction temperature was simulated and compared to the experimental results, as is depicted in Fig. 7. Within the investigated temperature range of 540–620 °C, the predicted selectivity and the yield at the oxygen-to-ethane molar

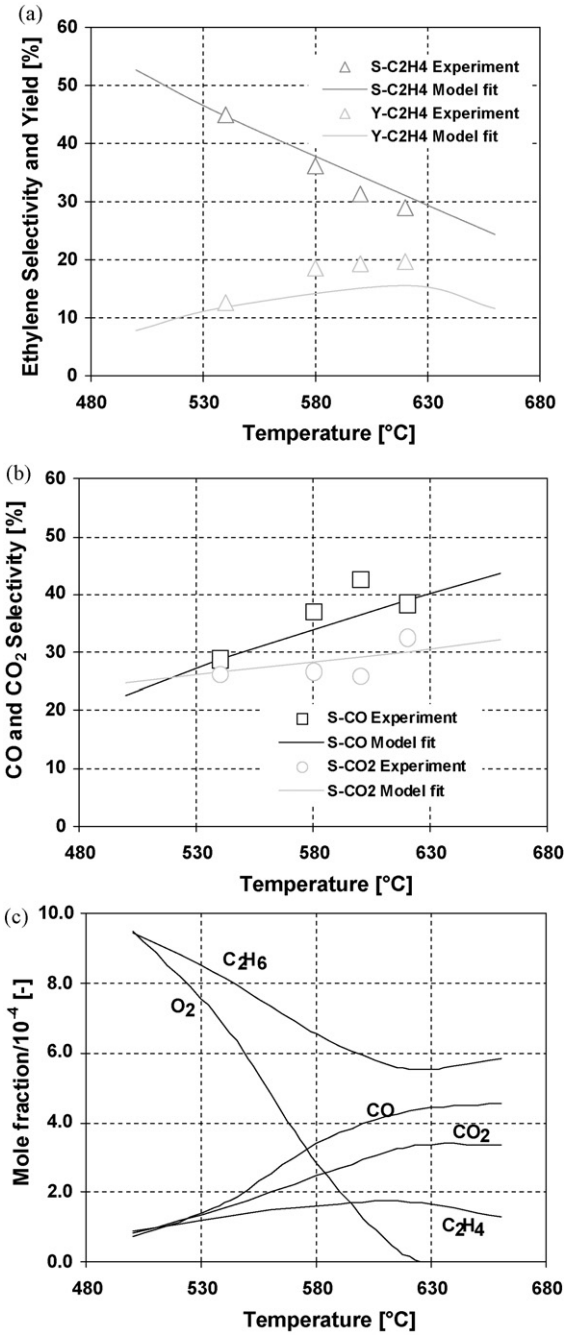

Fig. 7. Experimentally obtained and predicted ethylene selectivity and yield (a), and CO_x selectivities (b) as a function of the temperature during EMR operation (O_2/C_2H_6 = 1.25; W/F = 0.013 g min/cm^3). The predicted molar concentrations at temperatures between 500 and 660 °C (c). All predicted values calculated with the extended model including additional electrochemical side reactions.

ratio of 1.25 agreed well with the experimental results. Low temperatures favour the formation of ethylene, and the selectivity towards ethylene clearly decreased as a function of temperature, which was also well predicted by the model. At temperatures above 600 °C, the predicted ethylene yield declined, most likely due to the depletion of oxygen in the system. Expectedly, the CO_x selectivity was favoured at high temperatures due to the high activation energies. Fig. 7c illustrates the predicted mole fractions at the temperature range between 500 and 660 °C at the molar feed ratio 1.25. Oxygen is depleted at temperatures above 600 °C limiting the reactions.

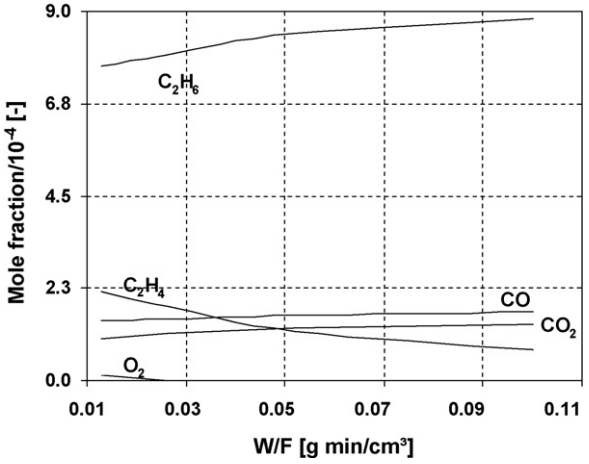

Fig. 8. Predicted molar concentrations at W/F ratio between 0.013 and 0.1 g min/cm^3 (T = 580 °C; O_2/C_2H_6 = 0.5). All predicted values calculated with the extended model including additional electrochemical side reactions.

Expectedly, at high temperatures, the concentrations of carbon oxides are high at molar ratio 1.25.

Fig. 8 shows the model estimations at temperature of 580 °C and O_2/C_2H_6 molar ratio of 0.5 for different W/F ratios. The W/F ratio was varied between values of 0.013 and 0.1 g min/cm^3 (resp. 100–13 ml/min), and the current between 16 and 2.1 mA, in order to fix the oxygen/ethane feed ratio 0.5. Expectedly, the increase of the W/F ratio (lower flow rate) caused the ethane concentration to decrease and the concentration of the side reaction products to increase. The longer residence time of the desired intermediate product ethylene in the anodic compartment caused its further conversion to CO and CO_2. Consequently, the ethylene concentration decreased steadily with increasing W/F ratio.

6. Conclusions

A mathematical model for an electrochemical membrane reactor applied for the ODH of ethane to ethylene was developed. Experimental data for the EMR and PBR operation modes were analysed for the identification of the unknown kinetic parameters of the electrochemical reactions and the VO_x/γ-Al_2O_3 catalysed reactions. The EMR conditions were not satisfactorily predicted by the simple model, where the release of molecular oxygen at the membrane–electrode interface was assumed to be the only electrochemical reaction on the anodic side. The electrochemical oxidation of ethylene to CO and CO_2 under the EMR operation mode was also considered in the model, leading to a significant improvement in the model predictions. The electrochemically induced effects also reported by Ye et al. [28], who investigated electrochemical butane oxidation to maleic anhydride with an identical electrochemical membrane reactor, were also confirmed in the present investigation.

Acknowledgement

The financial support for the research group No. 447 “Membrane supported reaction engineering” from the German Research Foundation is gratefully acknowledged.

References

[1] K. Weissermehl, H.-J. Arpe, Industrial Organic Chemistry, VCH, Weinheim, 2003.
[2] F. Cavani, F. Trifiro, Selective oxidation of light alkanes: interaction between the catalyst and the gas phase on different classes of catalytic materials, Catal. Today 51 (1999) 561–580.

[3] E. Heracleous, A.A. Lemonidou, Ni-Nb-O mixed oxides as highly active and selective catalysts for ethene production via ethane oxidative dehydrogenation, Part I: characterization and catalytic performance, J. Catal. 237 (2006) 162–174.
[4] E. Heracleous, M. Machli, A.A. Lemonidou, L.A. Vasalos, Oxidative dehydrogenation of ethane and propane over vanadia and molybdena supported catalysts, J. Mol. Catal. A-Chem. 232 (2005) 29–39.
[5] P. Botella, E. Garcia-Gonzalez, A. Dejoz, J.M.L. Nieto, M.I. Vazquez, J. Gonzalez-Calbet, Selective oxidative dehydrogenation of ethane on MoVTeNbO mixed metal oxide catalysts, J. Catal. 225 (2004) 428–438.
[6] B. Solsona, A. Dejoz, T. Garcia, P. Concepcion, J.M. Lopez Nieto, M.I. Vazquez, M.T. Navarro, Molybdenum-vanadium supported on mesoporous alumina catalysts for the oxidative dehydrogenation of ethane, Catal. Today 117 (2006) 228–233.
[7] A. Klisinska, K. Samson, I. Gressel, B. Grzybowska, Effect of additives on properties of V2O5/SiO2 and V2O5/MgO catalysts. I. Oxidative dehydrogenation of propane and ethane, Appl. Catal. A: Gen. 309 (2006) 10–16.
[8] F. Klose, T. Wolff, H. Lorenz, A. Seidel-Morgenstern, Y. Suchorski, M. Piórkowska, H. Weiss, Active species on γ-alumina-supported vanadia catalysts: nature and reducibility, J. Catal. 247 (2007) 176–193.
[9] M.E. Harlin, V.M. Niemi, A.O.I. Krause, Alumina-supported vanadium oxide in the dehydrogenation of butanes, J. Catal. 195 (2000) 67–78.
[10] J.M. Lopez Nieto, J. Soler, P. Concepcion, J. Herguido, M. Menendez, J. Santamaria, Oxidative dehydrogenation of alkanes over V-based catalysts: influence of redox properties on catalytic performance, J. Catal. 185 (1999) 324–332.
[11] M.V. Martinez-Huerta, X. Gao, H. Tian, I.E. Wachs, J.L.G. Fierro, M.A. Banares, Oxidative dehydrogenation of ethane to ethylene over alumina-supported vanadium oxide catalysts: relationship between molecular structures and chemical reactivity, Catal. Today 118 (2006) 279–287.
[12] F. Klose, T. Wolff, S. Thomas, A. Seidel-Morgenstern, Operation modes of packed-bed membrane reactors in the catalytic oxidation of hydrocarbons, Appl. Catal. A: Gen. 257 (2004) 193–199.
[13] D. Ahchieva, M. Peglow, S. Heinrich, L. Mörl, T. Wolff, F. Klose, Oxidative dehydrogenation of ethane in a fluidized bed membrane reactor, Appl. Catal. A: Gen. 296 (2005) 176–185.
[14] K. Sundmacher, L. Rihko-Struckmann, V. Galvita, Solid electrolyte membrane reactors: status and trends, Catal. Today 104 (2005) 185–199.
[15] K. Takehira, T. Komatsu, N. Sakai, H. Kajioka, S. Hamakawa, T. Shishido, T. Kawabata, K. Takaki, Oxidation of C_2–C_4 hydrocarbons over MoO_3 and V_2O_5 supported on a YSZ-aided membrane reactor, Appl. Catal. A: Gen. 273 (2004) 133–141.
[16] Y. Ye, L. Rihko-Struckmann, B. Munder, H. Rau, K. Sundmacher, Feasibility of an electrochemical membrane reactor for the partial oxidation of *n*-butane to maleic anhydride, Ind. Eng. Chem. Res. 43 (2004) 4551–4558.
[17] L. Chalakov, L.K. Rihko-Struckmann, B. Munder, K. Sundmacher, Feasibility study of the oxidative dehydrogenation of ethane in an electrochemical packed bed membrane reactor, Ind. Eng. Chem. Res. 46 (2007) 8665–8673.
[18] R. Grabowski, Kinetics of oxidative dehydrogenation of C_2–C_3 alkanes on oxide catalysts, Catal. Rev. 48 (2006) 199–268.
[19] S.T. Oyama, A.A. Middlebrook, G.A. Somorjai, Kinetics of ethane oxidation on vanadium oxide, J. Phys. Chem. 94 (1990) 5029–5033.
[20] R. Grabowski, J. Sloczynski, Kinetics of oxidative dehydrogenation of propane and ethane on VO_x/SiO_2 pure and with potassium additive, Chem. Eng. Process. 44 (2005) 1082–1093.
[21] J. Le Bars, J.C. Vedrine, A. Auroux, S. Trautmann, M. Baers, Oxidative dehydrogenation of ethane over V_2O_5/γ-Al_2O_3 catalysts, Appl. Catal. 88 (1992) 179–187.
[22] T.V.M. Rao, G. Deo, Ethane and propane oxidation over supported V_2O_5/TiO_2 catalysts: analysis of kinetic parameters, Ind. Eng. Chem. Res. 46 (2007) 70–79.
[23] F. Klose, M. Joshi, C. Hamel, A. Seidel-Morgenstern, Selective oxidation of ethane over a VO_x/γ-Al_2O_3 catalyst—investigation of the reaction network, Appl. Catal. A: Gen. 260 (2004) 101–110.
[24] B. Munder, L. Rihko-Struckmann, K. Sundmacher, Solid electrolyte membrane reactor for controlled partial oxidation of hydrocarbons: model and experimental validation, Catal. Today 104 (2005) 138–148.
[25] B. Munder, Y. Ye, L. Rihko-Struckmann, K. Sundmacher, Steady-state and forced-periodic operation of solid electrolyte membrane reactors for selective oxidation of *n*-butane to maleic anhydride, Chem. Eng. Sci. 62 (2007) 5663–5668.
[26] A. Kröner, P. Holl, W. Marquardt, E.D. Gilles, DIVA—an open architecture for dynamic simulation, Comp. Chem. Eng. 14 (1990) 1289–1295.
[27] L. Chalakov, L. Rihko-Struckmann, B. Munder, H. Rau, K. Sundmacher, Reaction induced current generation by butane oxidation in high temperature electrochemical membrane reactor, Chem. Eng. J. 131 (2007) 15–22.
[28] Y. Ye, L. Rihko-Struckmann, B. Munder, K. Sundmacher, Partial oxidation of *n*-butane in a solid electrolyte membrane reactor—influence of electrochemical oxygen pumping, J. Electrochem. Soc. 153 (2) (2006) D21–D29.
[29] J. Rutman, I. Riess, Placement of reference electrode in solid electrolyte cells, Electrochim. Acta 52 (2007) 6073–6083.
[30] M. Ni, M. Leung, D. Leung, Parametric study of solid oxide steam electrolyzer for hydrogen production, Int. J. Hydrogen Energy 32 (2007) 2305–2313.